NATIONAL ADVISORY COMMITTEE FOR AERONAUTICS

TECHNICAL NOTE 3155

IMPINGEMENT OF WATER DROPLETS ON NACA 65A004 AIRFOIL AT 8° ANGLE OF ATTACK

By Rinaldo J. Brun, Helen M. Gallagher, and Dorothea E. Vogt

Lewis Flight Propulsion Laboratory
Cleveland, Ohio



Washington
July 1954

NATIONAL ADVISORY COMMITTEE FOR AERONAUTICS

TECHNICAL NOTE 3155

IMPINGEMENT OF WATER DROPLETS ON NACA 65A004 AIRFOIL AT 8° ANGLE OF ATTACK

By Rinaldo J. Brun, Helen M. Gallagher, and Dorothea E. Vogt

SUMMARY

The trajectories of droplets in the air flowing past an NACA 65A004 airfoil at an angle of attack of 8° were determined. The amount of water in droplet form impinging on the airfoil, the area of droplet impingement, and the rate of droplet impingement per unit area on the airfoil surface were calculated from the trajectories and presented to cover a large range of flight and atmospheric conditions. These impingement characteristics are compared briefly with those previously reported for the same airfoil at an angle of attack of 4°.

INTRODUCTION

The data presented herein are a continuation of the study reported in reference 1 on the impingement of cloud droplets on a low-drag, thin airfoil. The airfoil studied in both the reference cited and in this report is a 4-percent-thick symmetrical NACA 65A004 airfoil. In reference 1 the impingement characteristics of the airfoil were reported with the airfoil set at an angle of attack of 4°; whereas, the data herein apply for an angle of attack of 8°. The data calculated for 8° angle of attack, along with those data for 4° presented in reference 1, permit the evaluation of the impingement characteristics for circling, landing, and some types of flight plans for pursuit or fighter aircraft.

The trajectories of atmospheric water droplets about an NACA 65A004 airfoil at 8° angle of attack at subsonic velocities were calculated with the aid of a differential analyzer at the NACA Lewis laboratory. From the computed trajectories, the rate, distribution, and surface extent of impinging water were obtained and summarized in this report.

SYMBOLS

The following symbols are used in this report:

d droplet diameter, microns (micron = 3.28×10^{-6} ft)

K inertia parameter, $1.704 \times 10^{-12} \frac{d^2 U}{\mu L}$, dimensionless (the density of water, 1.94 slugs/cu ft, is included in the constant)

L airfoil chord length, ft

Re_0 free-stream Reynolds number with respect to droplet, $4.813 \times 10^{-6} \frac{d \rho_a U}{\mu}$, dimensionless

S distance on surface of airfoil measured from leading-edge chord point, ratio to chord length

U flight speed, mph

u local air velocity, ratio to free-stream velocity

W rate of water impingement per unit span of airfoil, lb/(hr)(ft span)

W_m rate of total water impingement per unit span of airfoil, lb/(hr)(ft span)

W_β local rate of water impingement, lb/(hr)(sq ft)

w liquid-water content in cloud, g/cu m

x,y rectangular coordinates, ratio to chord length

β local impingement efficiency, $\frac{dy_0}{dS}$, dimensionless

μ viscosity of air, slugs/(ft)(sec)

ρ_a density of air, slugs/cu ft

Subscripts:

l lower airfoil surface

s airfoil surface

u upper airfoil surface

0 free stream

RESULTS AND DISCUSSION

In order to obtain the extent of impingement and the rate of droplet impingement per unit area on the airfoil, the cloud droplet trajectories with respect to the airfoil were determined. The method for calculating the droplet trajectories is described in reference 2. A solution of the differential equations that describe the droplet motion was obtained with the use of the mechanical analog (described in ref. 3) based on the principle of a differential analyzer. The air-flow field around the airfoil was obtained by the vortex substitution method described in reference 2, except that, for the NACA 65A004 airfoil, the velocities at the surface of the airfoil were calculated by the method described in reference 4, whereas the surface velocities on the 65_1-212 and 65_1-208 airfoils discussed in reference 2 were obtained from wind-tunnel measurements of the pressure coefficients. The values of the surface velocities for the 65A004 airfoil were calculated by the Douglas Aircraft Corporation for the Lewis laboratory (see fig. 1). Although the droplet trajectories were calculated for an incompressible flow field, the results of the calculations can be applied up to the flight critical Mach number (ref. 5).

The geometric chord line of the airfoil is oriented at an angle of 8° with the x-axis of the rectangular coordinate system, and the leading edge is placed at the origin of the coordinates, as shown in figure 2. The airfoil orientation presented in references 1 and 2 is retained herein, except for the magnitude of the angle of attack. At an infinite distance ahead of the airfoil, the uniform air flow carrying the cloud droplets is assumed to be approaching the airfoil from the negative x-direction and parallel to the x-axis. All distances are dimensionless, because they are ratios of the respective actual distance to the airfoil chord length L.

Rate of Water Interception

The rate of total water interception, in pounds per hour per foot of wing span, is determined by the tangent droplet trajectories (fig. 2), by the speed of the aircraft, and by the liquid-water content in the cloud. The flight speed and size of the airfoil, as well as the droplet size in the cloud, are the principal variables that affect the spacing between the two tangent trajectories. The amount of water that strikes the airfoil is proportional to the spacing $y_{0,u} - y_{0,l}$, and the rate of total water interception per unit span of the airfoil on that portion of the airfoil surface bounded by the upper and lower tangent trajectories can be calculated from the relation

$$W_m = 0.33UwL(y_{0,u} - y_{0,l}) \tag{1}$$

The values of $y_{0,u} - y_{0,l}$ are given in figure 3 in terms of the reciprocal of the inertia parameter $1/K$ and the free-stream Reynolds number Re_0. The inertia parameter K is a measure of the droplet size, the flight speed and size of the airfoil, and the viscosity of the air through the relation

$$K = 1.704 \times 10^{-12} \frac{d^2 U}{\mu L} \tag{2}$$

The density of water and the acceleration of gravity, which are expressed as part of the conversion factor, are 62.4 pounds per cubic foot and 32.17 feet per second per second, respectively. The free-stream Reynolds number is defined with respect to the droplet as

$$Re_0 = 4.813 \times 10^{-6} \frac{d \rho_a U}{\mu} \tag{3}$$

A graphical procedure for determining values of the dimensionless parameters K and Re_0 in terms of airplane speed, chord length, altitude, and droplet size is presented in appendix B of reference 2.

The variation of rate of water interception with airfoil speed is summarized for an altitude of 20,000 feet in figure 4, in which the ordinate W_m/w is the total rate of water impingement per foot span of airfoil per unit liquid-water content (g/cu m) in the cloud. Several chord lengths ranging in value from 2 feet to 20 feet are considered. The values in figure 4 are for flight through clouds composed of uniform droplets 15, 20, 30, and 40 microns in diameter. The values of W_m/w given in figure 4 are based on the most probable icing temperature as a function of altitude presented in figure 15 of reference 2. (The most probable icing temperature was obtained from approximately 300 icing observations in flights.) As shown in reference 2, a change in altitude of 10,000 feet will change the rate of water impingement by approximately 7 percent. The droplet size and the liquid-water content of clouds are seldom known with sufficient accuracy (ref. 3) to permit the rate of water impingement to be calculated within 10 percent; therefore, within practical limits of application, the results of figure 4 can be used over a wide range of altitudes (approx. $\pm$10,000 ft, see ref. 2).

The effect of wing taper can also be obtained from figure 4, provided that for each section of span considered the taper is small enough that two-dimensional flow over the section is approximated, as is mentioned in reference 2.

Extent of Impingement

The limit of impingement is determined by the point of tangency on the airfoil surface of the two tangent trajectories. The rearward limits of impingement on the upper surface are shown in figure 5(a), and on the lower surface in figure 5(b). The distances S_u and S_l are measured on the airfoil surface from the point of intersection of the geometric chord line with the leading edge (fig. 2) in terms of the chord length. The limits of impingement are given in figure 5 in terms of the reciprocal of the inertia parameter and free-stream Reynolds number.

At an angle of attack of 8° the extent of impingement on the upper surface is always less than 2 percent of chord ($S_u = 0.02$), which is the largest value possible for the extreme conditions where $1/K = 0$. The value of S_u for $1/K = 0$ was obtained from simple geometric relations. The remaining values of S_u presented in figure 5(a) were obtained from calculated trajectories. These calculated values may be quite inaccurate, because of the sharp-edged shape of the airfoil at the leading edge. The accuracy of determination of S_u is unimportant in an application to airfoil icing calculations, because all values of S_u must be less than 0.02. The estimated accuracy for the values given in figure 5(a) is ± 20 percent.

Nearly all the water impinging on the airfoil impinges on the lower surface between the leading-edge chord point and the lower limit given in figure 5(b). As was discussed in reference 1 for the NACA 65A004 airfoil at 4° angle of attack, the tangent trajectories approach the lower surface of this airfoil very gradually. This very gradual approach of the lower-surface tangent trajectories leads to uncertainties as to the location of the tangent point, and the values of S_l are therefore subject to individual interpretation. The uncertainties in the location of the tangent point can range from ± 4-percent chord at $1/K \simeq 1$ to ± 7 percent at $1/K \simeq 3$ and back to ± 4 percent at $1/K \simeq 100$. For the extreme case of $1/K = 0$, the impingement extends to the trailing edge of the airfoil section. The lower-surface limits are summarized in figure 6 for the same speeds, chord lengths, droplet sizes, and altitude given in figure 4.

Impingement Distribution on Surface

Trajectory starting ordinate as function of point of impact. - The manner in which water is distributed on the surface of an airfoil can be obtained if the starting point of a droplet trajectory is known with respect to the point of impingement on the surface. The starting

ordinate y_0 at infinity of any impinging trajectory, including trajectories bounded by the upper and lower tangent trajectories (fig. 1), can be found in figure 7 with respect to the point of impingement on the surface. The values for the starting and ending positions of the trajectories are shown in figure 7 for four values of free-stream Reynolds number. For each value of Re_0, curves for several values of $1/K$ are given.

The amount of water impinging between any two given points on the airfoil surface may be found by applying the results of figure 7 in the relation

$$W = 0.33UwL(y_{0,1} - y_{0,2}) \tag{4}$$

The values of $y_{0,u} - y_{0,l}$ obtained from the end points of each curve in figure 7 are the same as the values given in figure 3. The value of $y_{0,l}$ for $1/K = 0$ (not shown in fig. 7) is -0.139 at $S_l = 1.00229$ (airfoil trailing edge) for all values of Re_0.

Local rate of droplet impingement. - The local rate of droplet impingement per unit area of airfoil surface can be determined from the expression

$$W_\beta = 0.33Uw\frac{dy_0}{dS} = 0.33Uw\beta \tag{5}$$

which is related to equation (4), with proper consideration for the fact that y_0 and S are based on the wing chord L. The values of the local impingement efficiency β as a function of the airfoil distance S are given in figure 8. These values were obtained from the slopes of the curves in figure 7.

As is discussed in reference 1, the values of β (fig. 8) are very sensitive to the shape of the y_0 against S curves (fig. 7). Because of the geometry of the sharp-nosed NACA 65A004 airfoil and the manner in which the trajectories approach the airfoil surface, small errors in the calculated trajectories result in considerable error in the slopes of the curves of figure 7. The possible error in the values of β, due to the computational procedure, for surface positions other than near the stagnation point, is estimated in reference 1 to be somewhat less than ± 10 percent for the values reported therein. Because of improved techniques in the computational procedure, the values of β given in figure 8 herein are in error by somewhat less than ± 2 percent for surface positions other than within 1 percent of the surface distance where the peak

values of β occur. Since the total water impinging is directly related to

$$y_{0,u} - y_{0,l} = \int_{-S_l}^{S_u} \beta \, dS \tag{6}$$

a check on the computational accuracy of the values of β in figure 8 was also obtained by comparing the area under each β curve with the values of $y_{0,u} - y_{0,l}$ given in figure 3. The area values checked within $\pm$1.5 percent of the corresponding values for total water interception.

The accuracy in the maximum value of β is also improved in this report as compared with that reported in reference 1. The possible error was estimated to be $\pm$25 percent for the maximum values of β reported in the reference cited; whereas, the possible error in the maximum values of β given in figure 8 is estimated to be less than $\pm$12 percent. As was discussed in reference 2, this possible error is not considered very serious, because only a small portion of the total water impinging on the airfoil is involved in the error.

Comparison of Impingement at 8° with Impingement at 4° Angle of Attack

Rate of total water interception. - For all values of the reciprocal of inertia parameter and free-stream Reynolds number, the rate of total water interception is greater at an angle of attack of 8° than at an angle of attack of 4°. This comparison can be made between figure 3 of this report and figure 3 of reference 1. The comparison is summarized in the following table for conditions established at 300 miles per hour, a chord length of 9.4 feet, and an altitude of 10,000 feet:

Reciprocal of inertia parameter, 1/K	Droplet diameter, d, microns	Free-stream Reynolds number, Re_0	$y_{0,u} - y_{0,l}$ Angle of attack		Ratio of rate of total water at 8° to rate at 4°
			8°	4°	
1	80	594	0.099	0.053	1.87
10	25	190	.043	.021	2.05
100	8	59	.017	.005	3.40

The value of free-stream Reynolds number tabulated is the value obtained from equation (3) for the physical conditions established for this comparison.

Extent of impingement. - Although the limit of impingement on the upper surface is farther rearward for an angle of attack of 4° than for 8°, the total extent is very small in both cases. At 4° angle of attack S_u is always less than 0.02 for values of $1/K>1$. At 8° angle of attack S_u is always less than 0.01 for values of $1/K>1$.

The impingement on the lower surface extends back to the trailing edge at both angles of attack for $1/K = 0$. The lower-surface limit is summarized in the following table for the same flight and atmospheric conditions given in the preceding section on rate of total water interception:

Reciprocal of inertia parameter, $1/K$	Droplet diameter, d, microns	Free-stream Reynolds number, Re_0	Limit of impingement on lower surface, S_l	
			Angle of attack	
			8°	4°
1	80	594	0.74	0.53
10	25	190	.34	.17
100	8	59	.21	.03

Local rate of droplet impingement. - At a given point on the lower surface, the local rate of droplet impingement β is greater at an angle of attack of 8° than at 4°. For both 8° and 4°, the maximum rate of local impingement occurs between 0 and $S = 0.01$ on the lower surface. The peak values of β are higher at 8° than at 4°. At 8° angle of attack the peak values are between 0.8 and 1.0; whereas, at 4° the peak values are reported as low as 0.3 and none higher than 0.56. These large differences cannot all be accounted for by the possible estimated error in determining the peak values.

CONCLUDING REMARKS

The data presented herein apply directly to flights in clouds composed of droplets that are all uniform in size and to nonswept wings of high aspect ratio. A detailed procedure for weighting the impingement of droplets for flights in nonuniform clouds is presented in reference 3. A method for extending the impingement calculations for nonswept wings to swept wings is presented in reference 6. As is discussed in reference 5, the impingement results should be applicable for most engineering uses throughout the subsonic region, because the subsonic compressibility of air does not affect the droplet trajectories appreciably.

Lewis Flight Propulsion Laboratory
National Advisory Committee for Aeronautics
Cleveland, Ohio, May 20, 1954

REFERENCES

1. Brun, Rinaldo J., Gallagher, Helen M., and Vogt, Dorothea E.: Impingement of Water Droplets on NACA 65A004 Airfoil and Effect of Change in Airfoil Thickness from 12 to 4 Percent at 4° Angle of Attack. NACA TN 3047, 1953.

2. Brun, Rinaldo J., Gallagher, Helen M., and Vogt, Dorothea E.: Impingement of Water Droplets on NACA 65_1-208 and 65_1-212 Airfoils at 4° Angle of Attack. NACA TN 2952, 1953.

3. Brun, Rinaldo J., and Mergler, Harry W.: Impingement of Water Droplets on a Cylinder in an Incompressible Flow Field and Evaluation of Rotating Multicylinder Method for Measurement of Droplet-Size Distribution, Volume-Median Droplet Size, and Liquid-Water Content in Clouds. NACA TN 2904, 1953.

4. Theodorsen, T., and Garrick, I. E.: General Potential Theory of Arbitrary Wing Sections. NACA Rep. 452, 1943.

5. Brun, Rinaldo J., Serafini, John S., and Gallagher, Helen M.: Impingement of Cloud Droplets on Aerodynamic Bodies as Affected by Compressibility of Air Flow Around the Body. NACA TN 2903, 1953.

6. Dorsch, Robert G., and Brun, Rinaldo J.: A Method for Determining Cloud-Droplet Impingement on Swept Wings. NACA TN 2931, 1953.

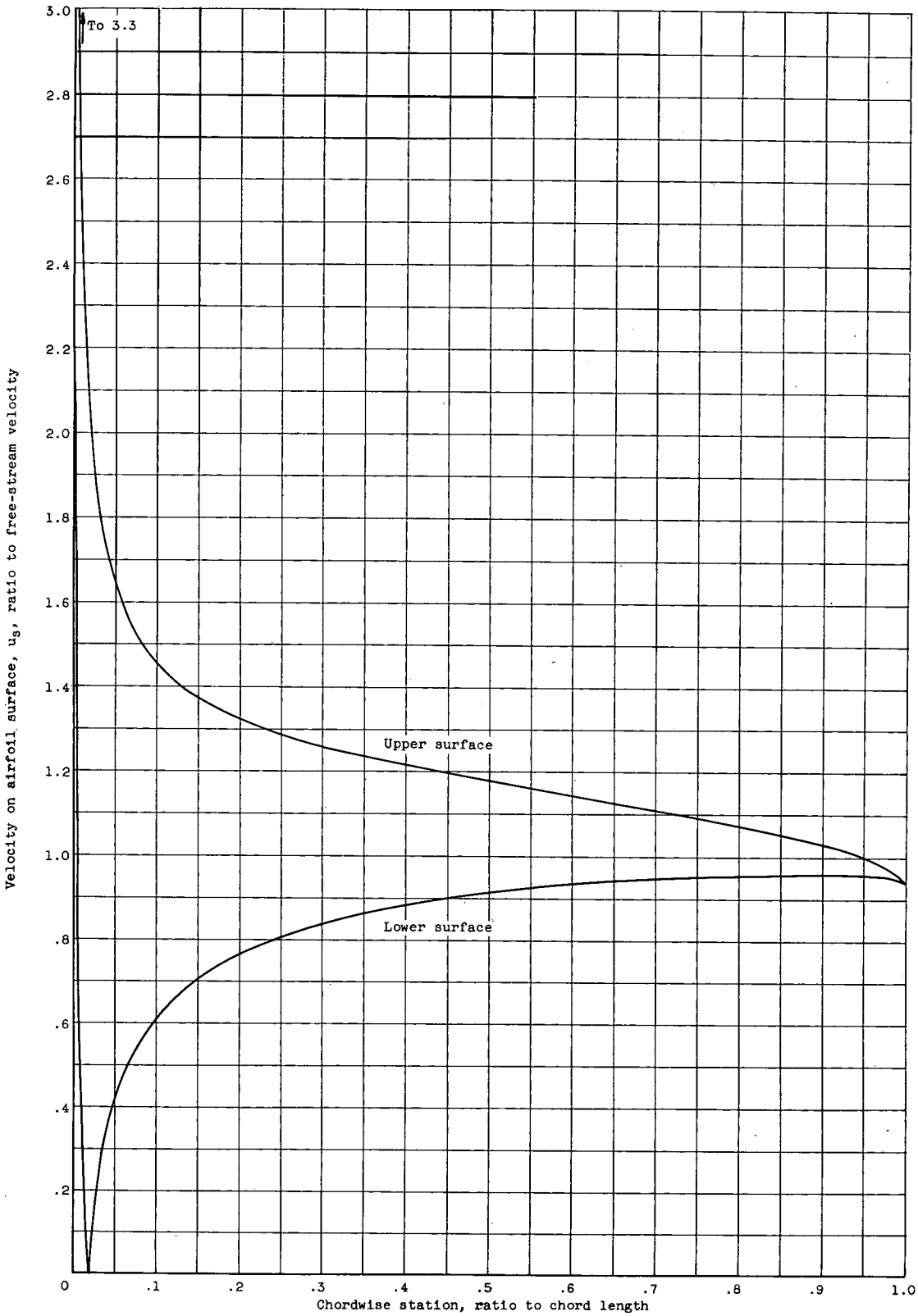


Figure 1. - Velocities on surface of 65A004 airfoil. Angle of attack, 8°; incompressible flow field.

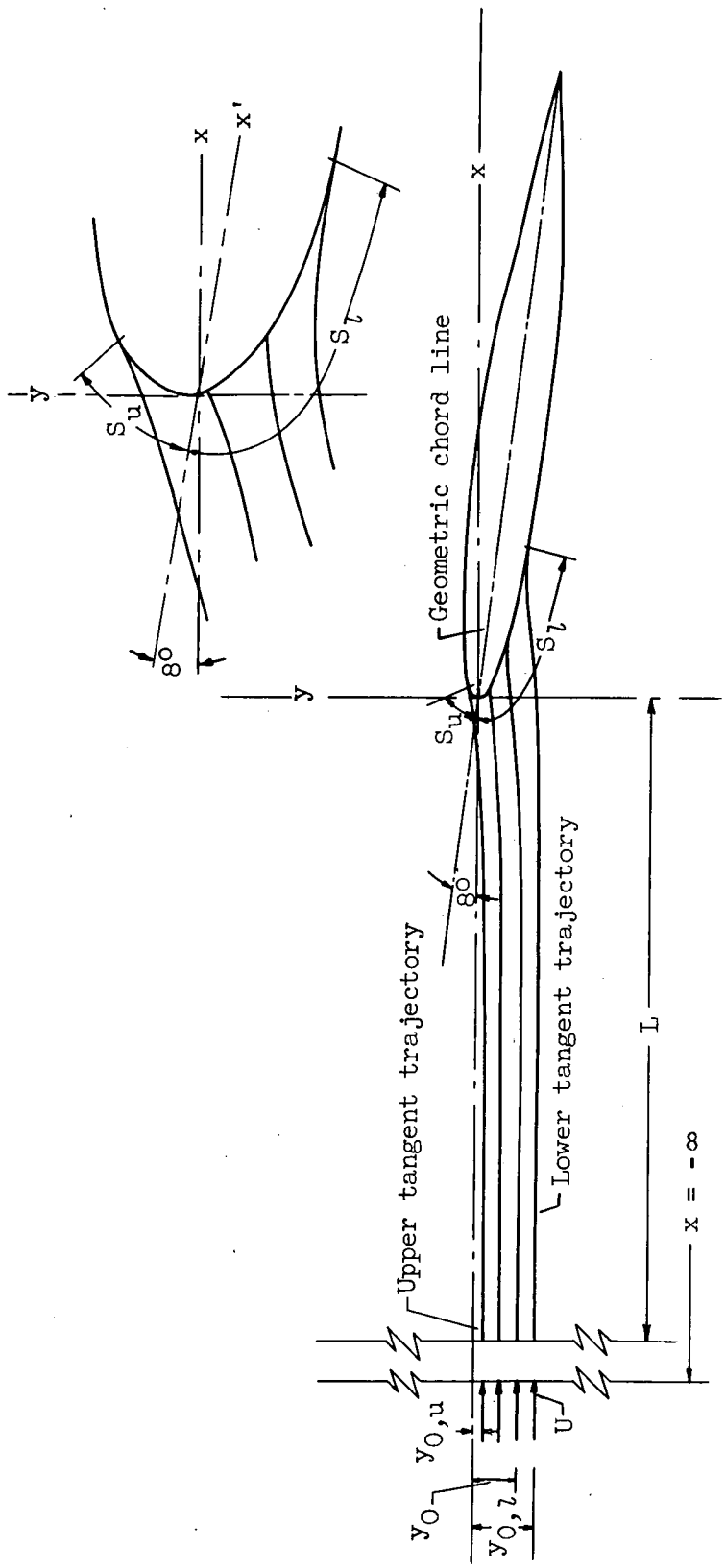


Figure 2. - Droplet trajectories with respect to airfoil.

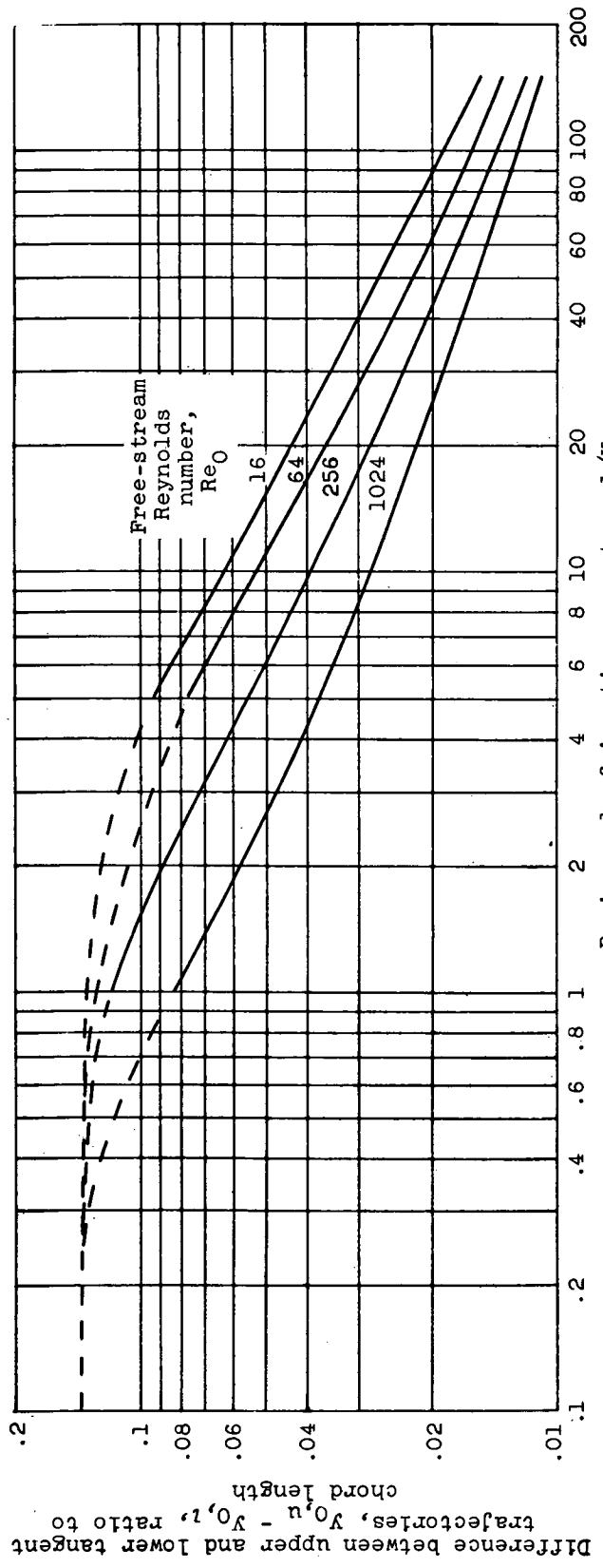
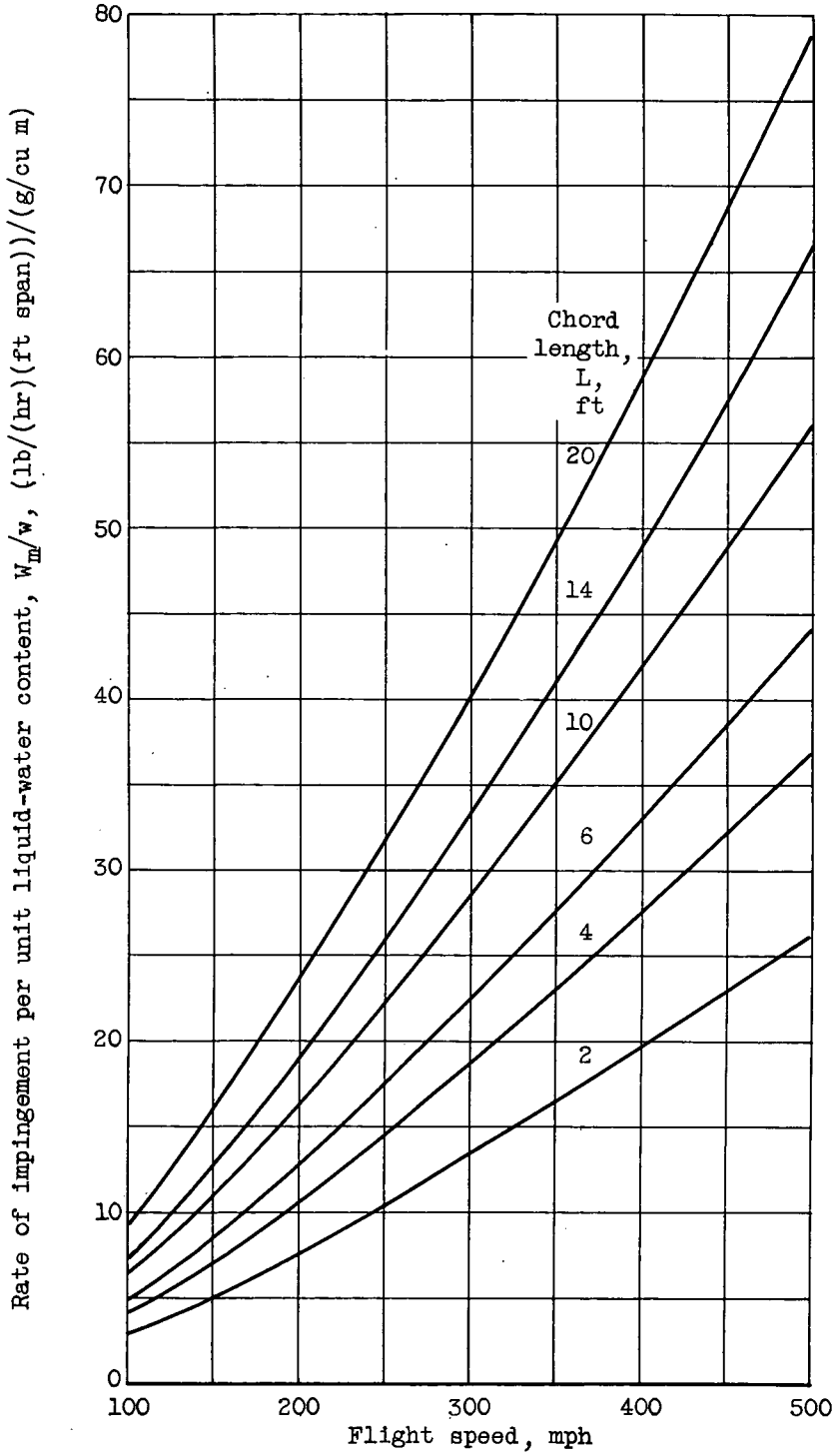
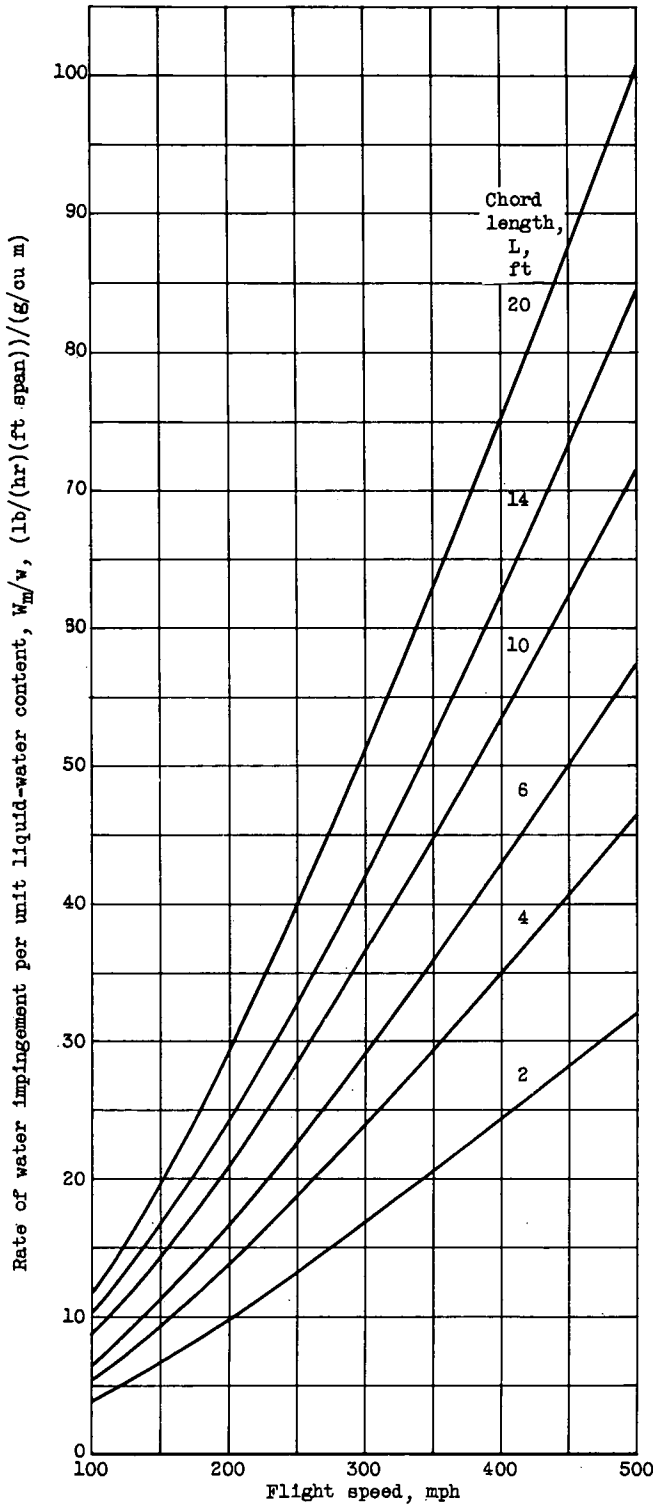


Figure 3. - Difference between upper and lower trajectories at free-stream conditions for 65A004 airfoil. Angle of attack, 8°.



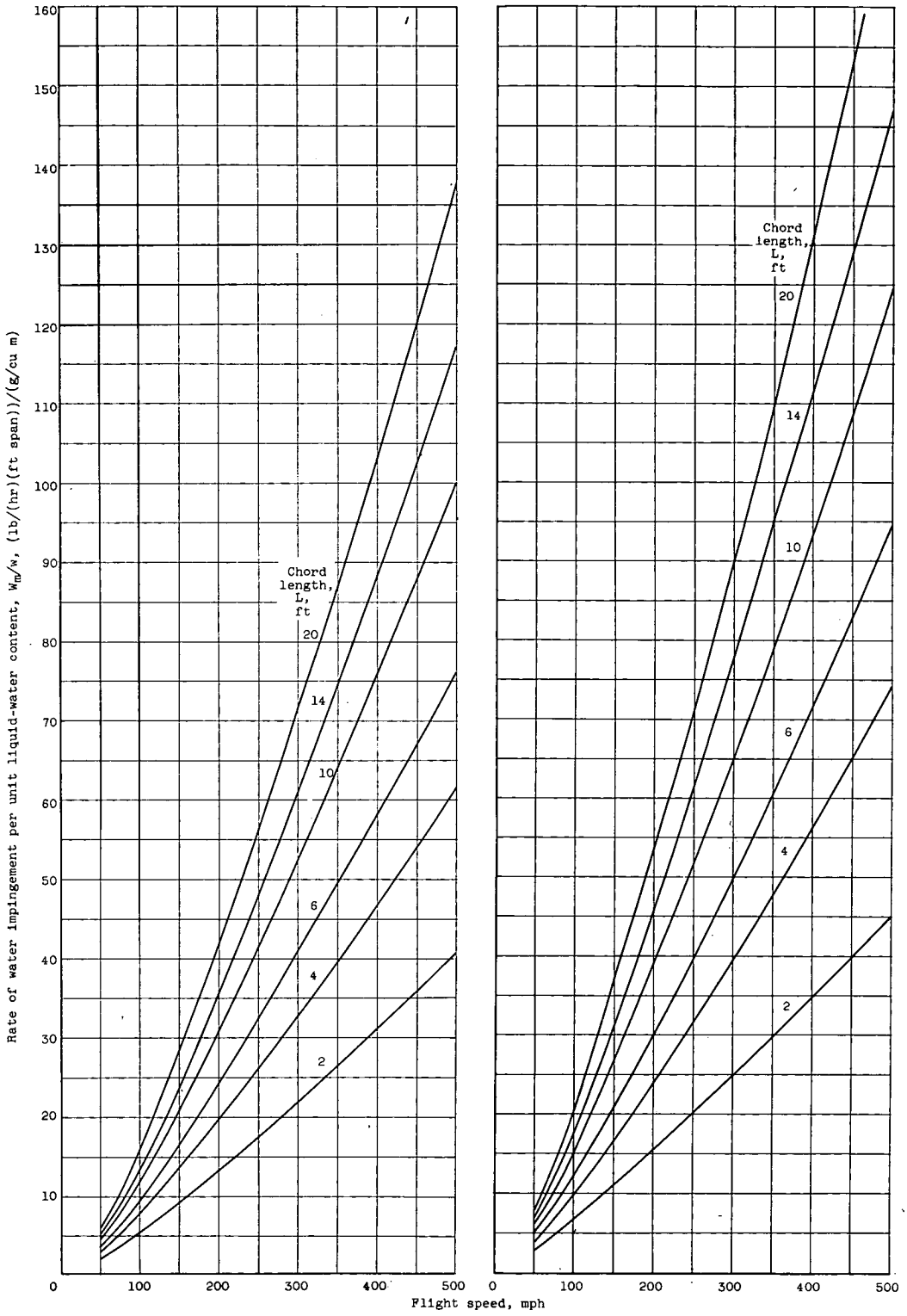
(a) Droplet size, 15 microns.

Figure 4. - Total rate of water impingement on 65A004 airfoil. Angle of attack, 8°; altitude, 20,000 feet; most probable icing temperature, -11° F.



(b) Droplet size, 20 microns.

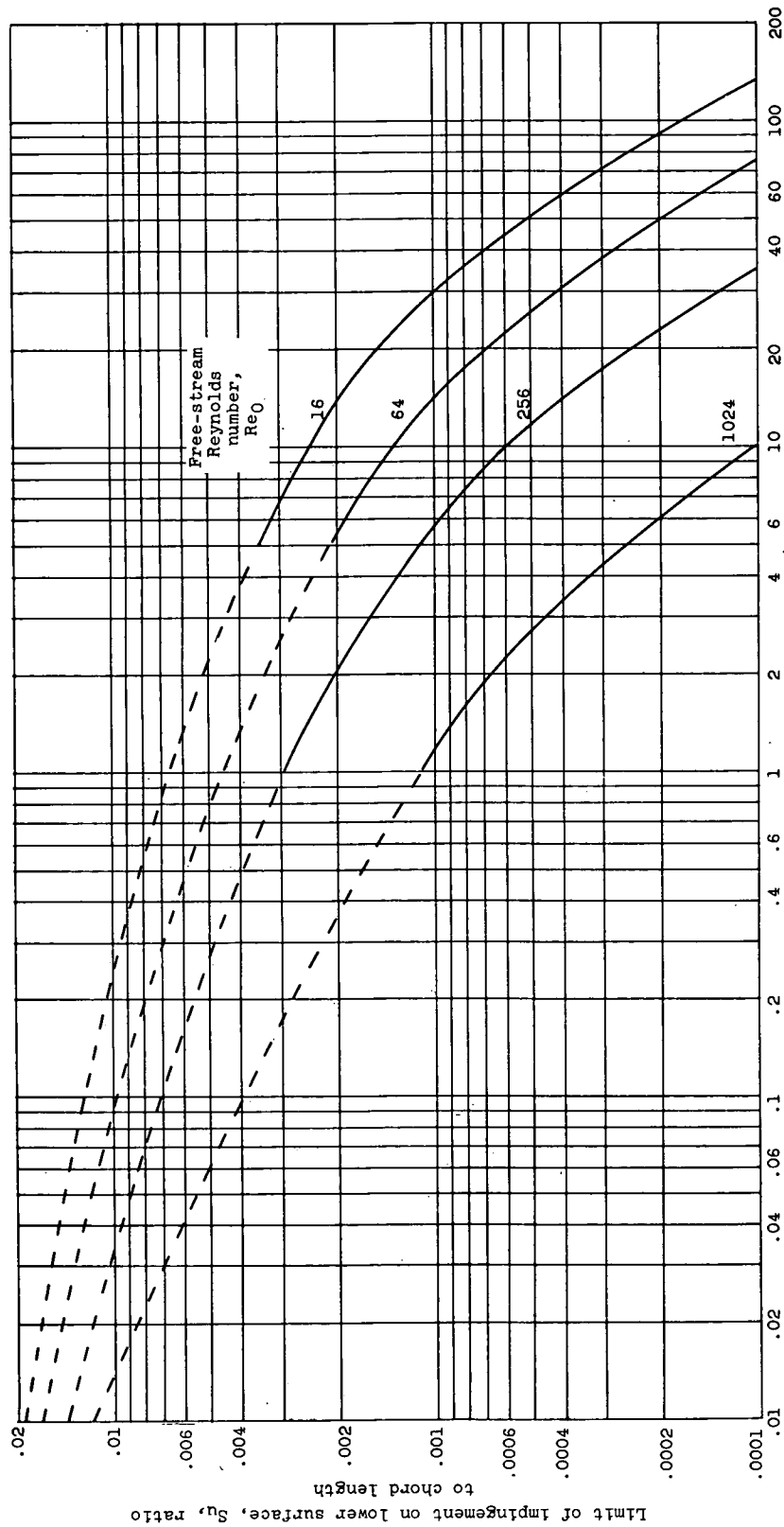
Figure 4. - Continued. Total rate or water impingement on 65A004 airfoil. Angle of attack, 8°; altitude, 20,000 feet; most probable icing temperature, -11° F.



(c) Droplet size, 30 microns.

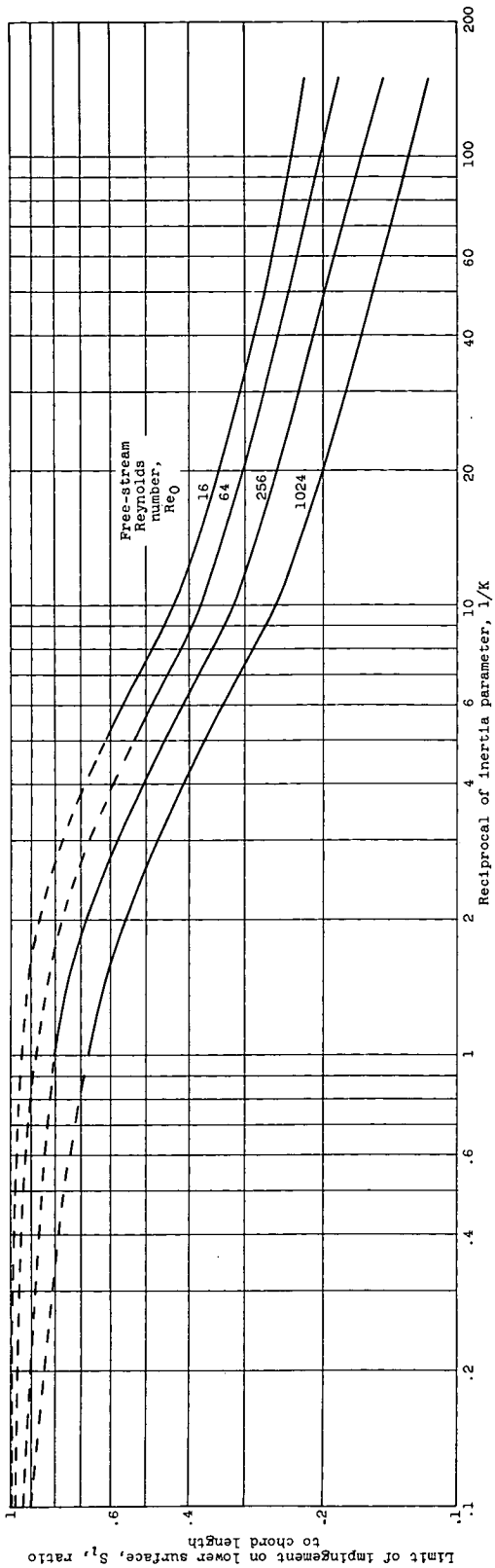
(d) Droplet size, 40 microns.

Figure 4. - Concluded. Total rate of water impingement on 65A004 airfoil. Angle of attack, 8°; altitude, 20,000 feet; most probable icing temperature, -11° F.



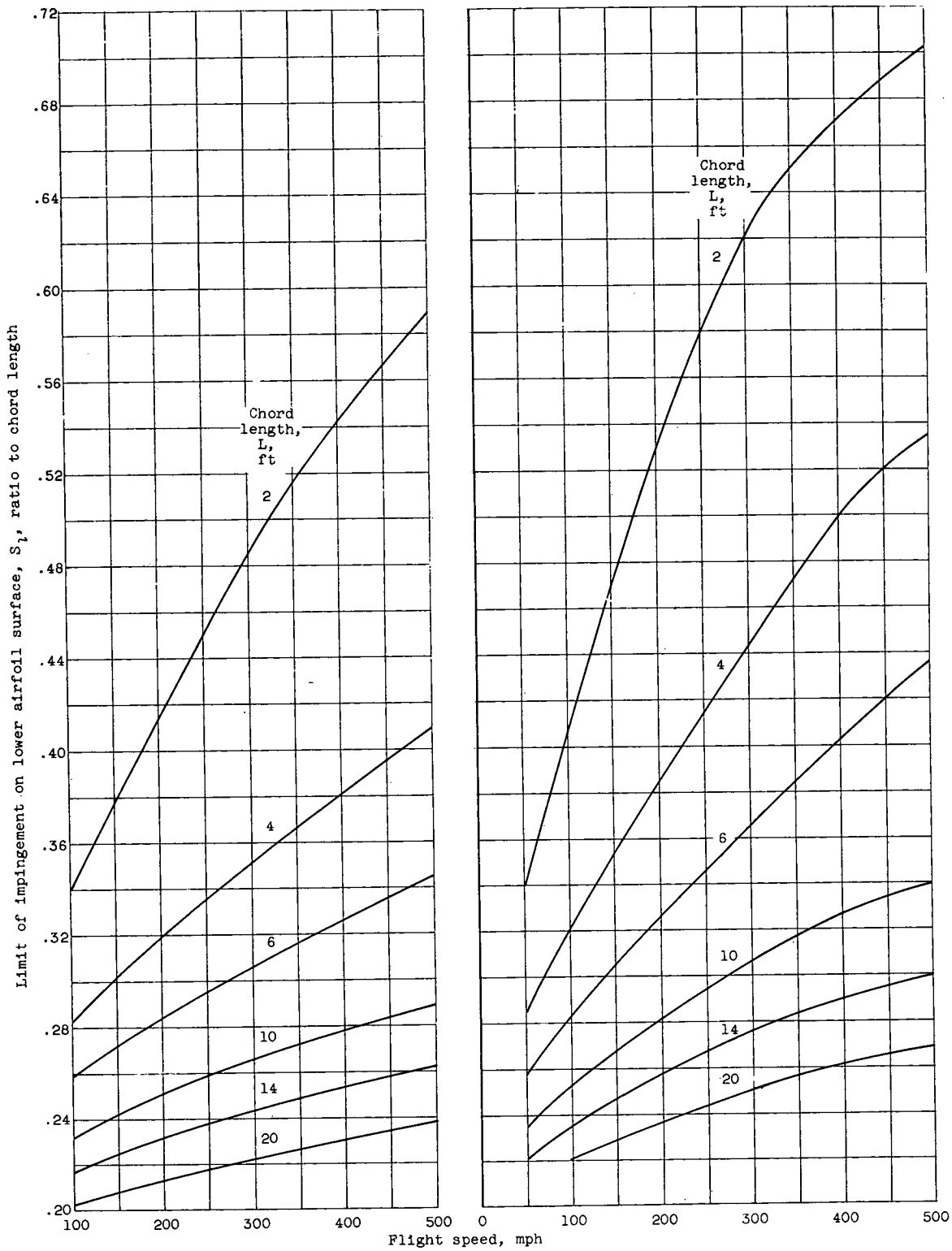
(a) Upper surface.

Figure 5. - Limit of impingement on surface of 65A004 airfoil. Angle of attack, 8°.



(b) Lower surface.

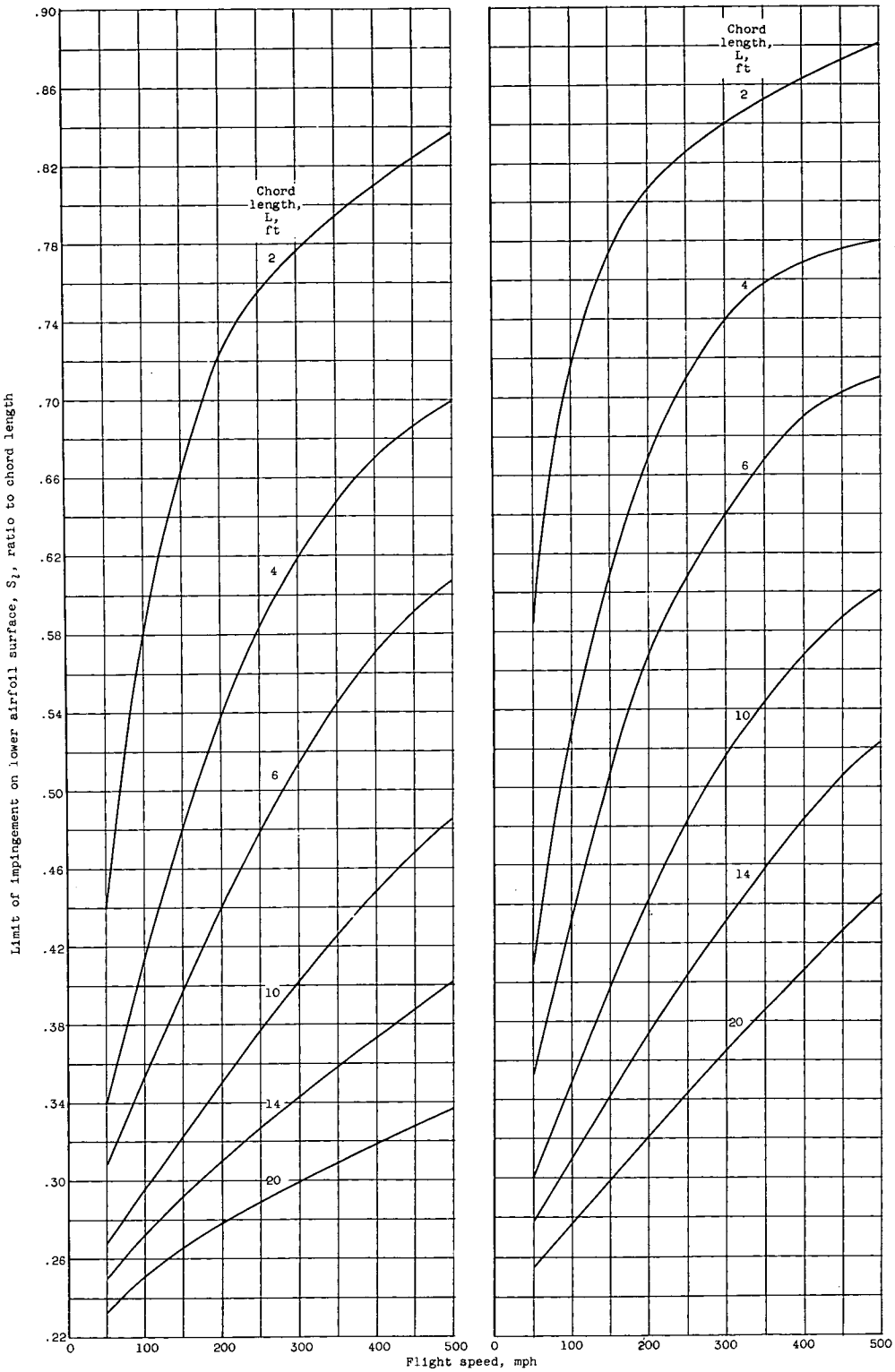
Figure 5. - Concluded. Limit of impingement on surface of 65A004 airfoil. Angle of attack, 8°.



(a) Droplet size, 15 microns.

(b) Droplet size, 20 microns.

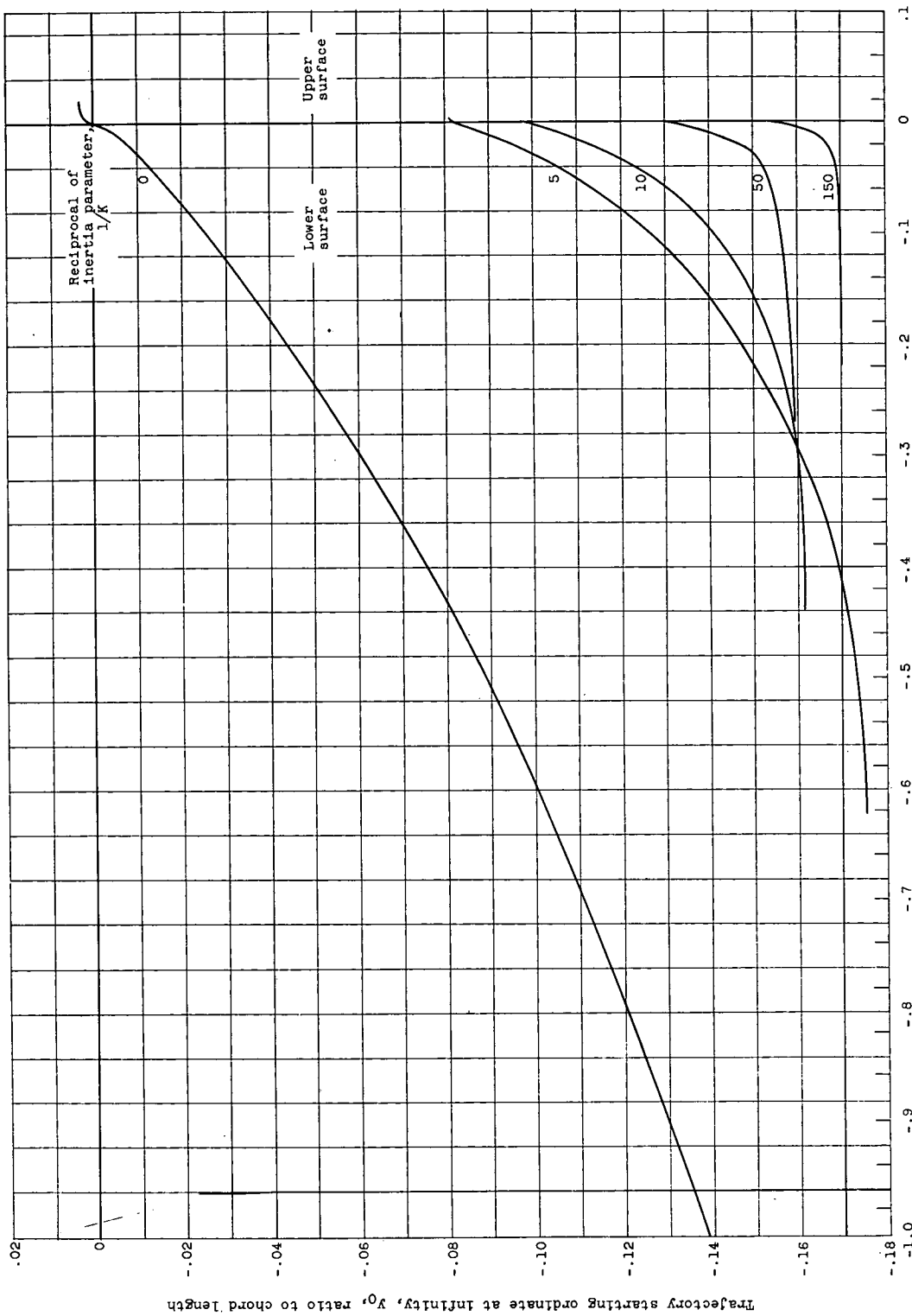
Figure 6. - Limit of impingement along lower surface of 65A004 airfoil. Altitude, 20,000 feet; angle of attack, 8°; most probable icing temperature, -11° F.



(c) Droplet size, 30 microns.

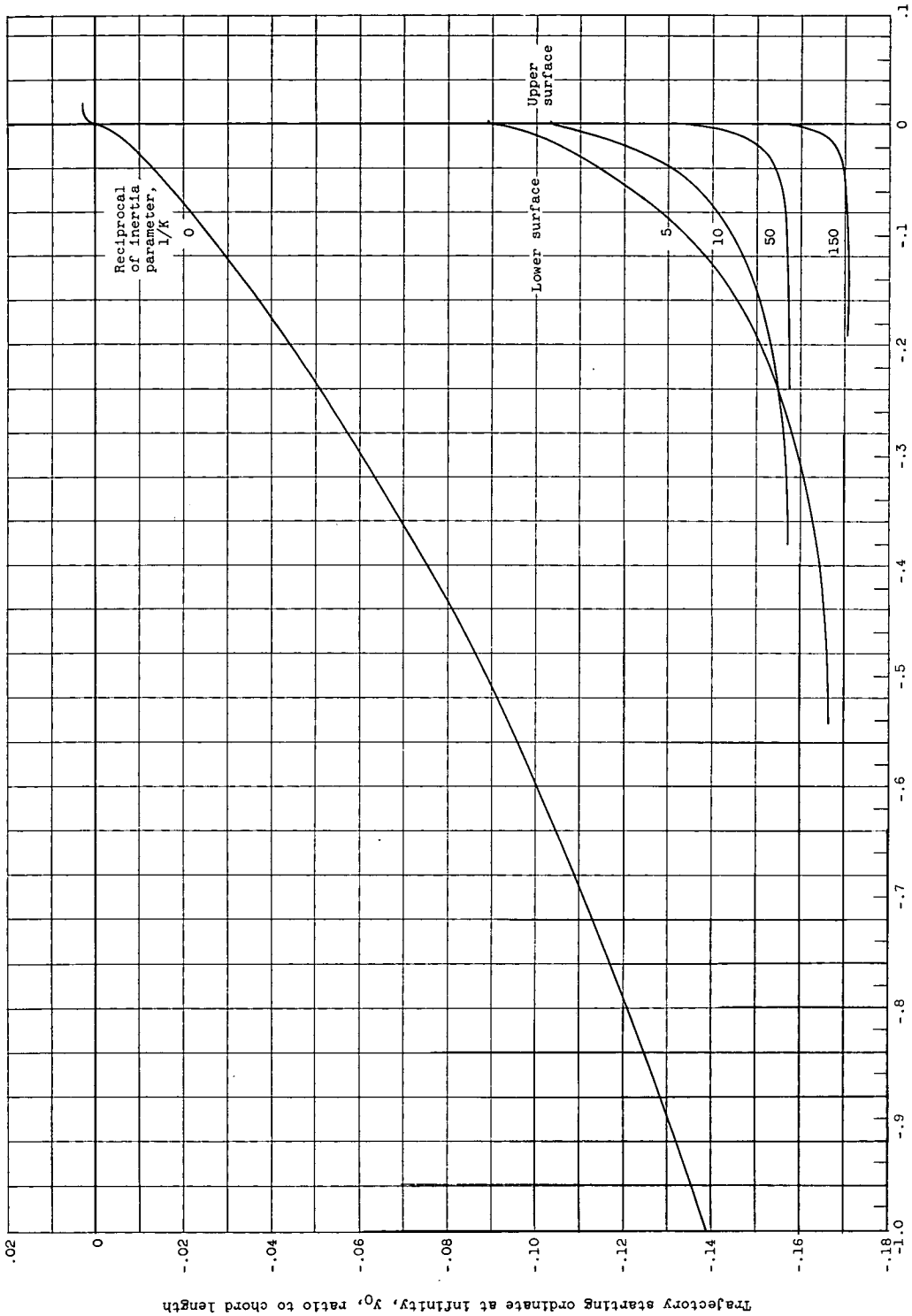
(d) Droplet size, 40 microns.

Figure 6. - Concluded. Limit of impingement along lower surface of 65A004 airfoil. Altitude, 20,000 feet; angle of attack, 8°; most probable icing temperature, -11° F.



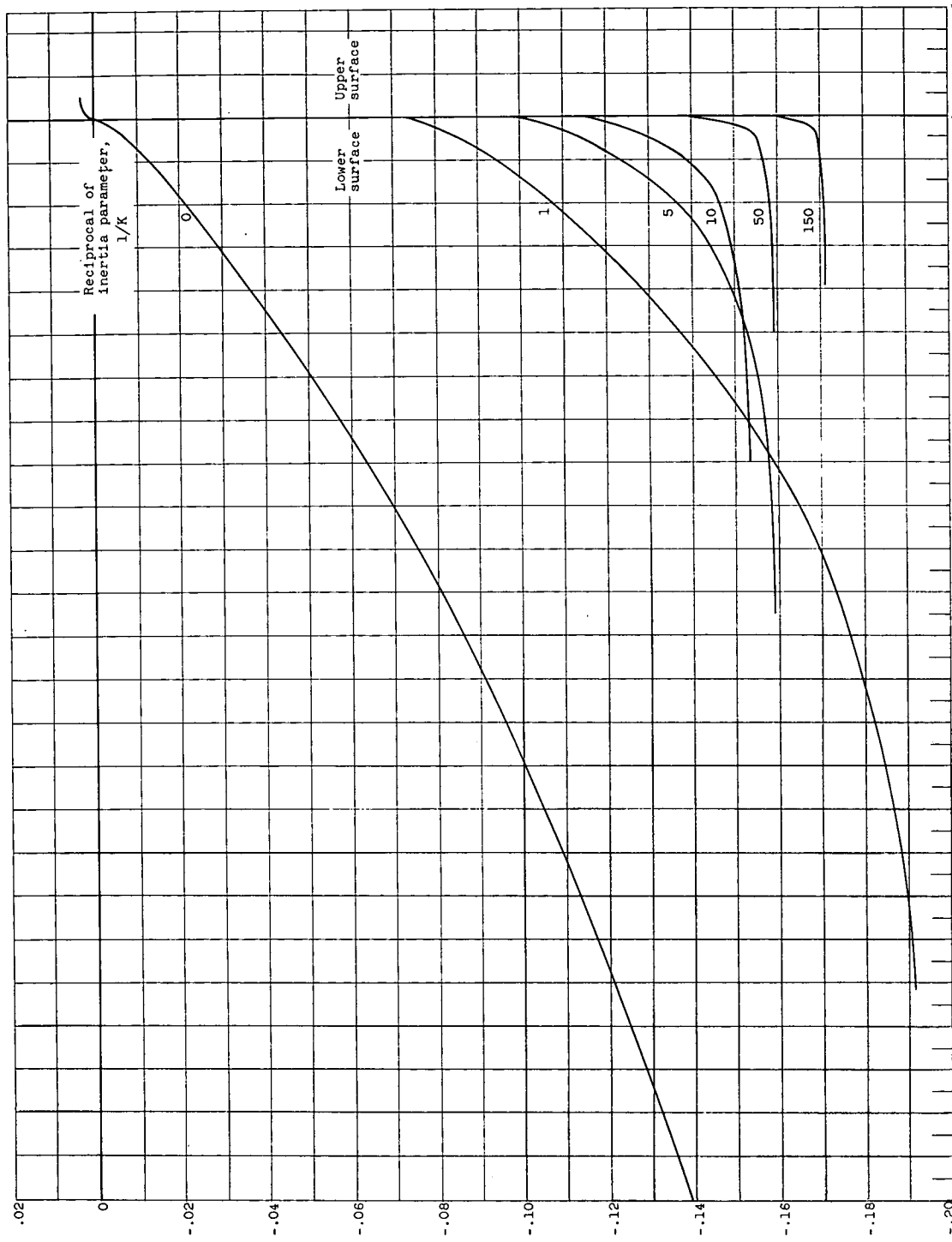
(a) Free-stream Reynolds number, 16.

Figure 7. - Trajectory starting ordinates as function of point of impingement on surface of 65A004 airfoil. Angle of attack, 8°.



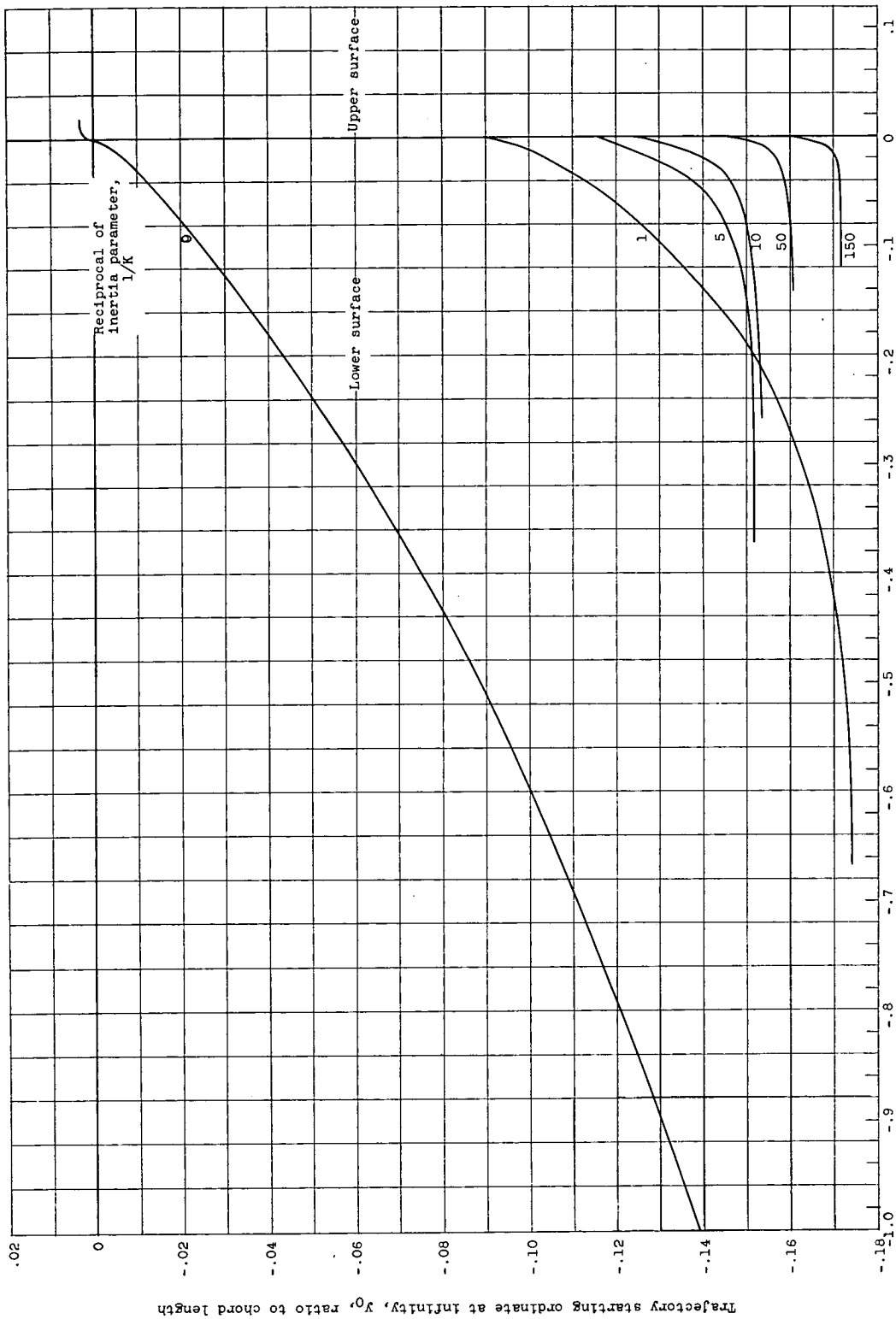
(b) Free-stream Reynolds number, 64.

Figure 7. - Continued. Trajectory starting ordinates as function of point of impingement on surface of 65A004 airfoil. Angle of attack, 8°.



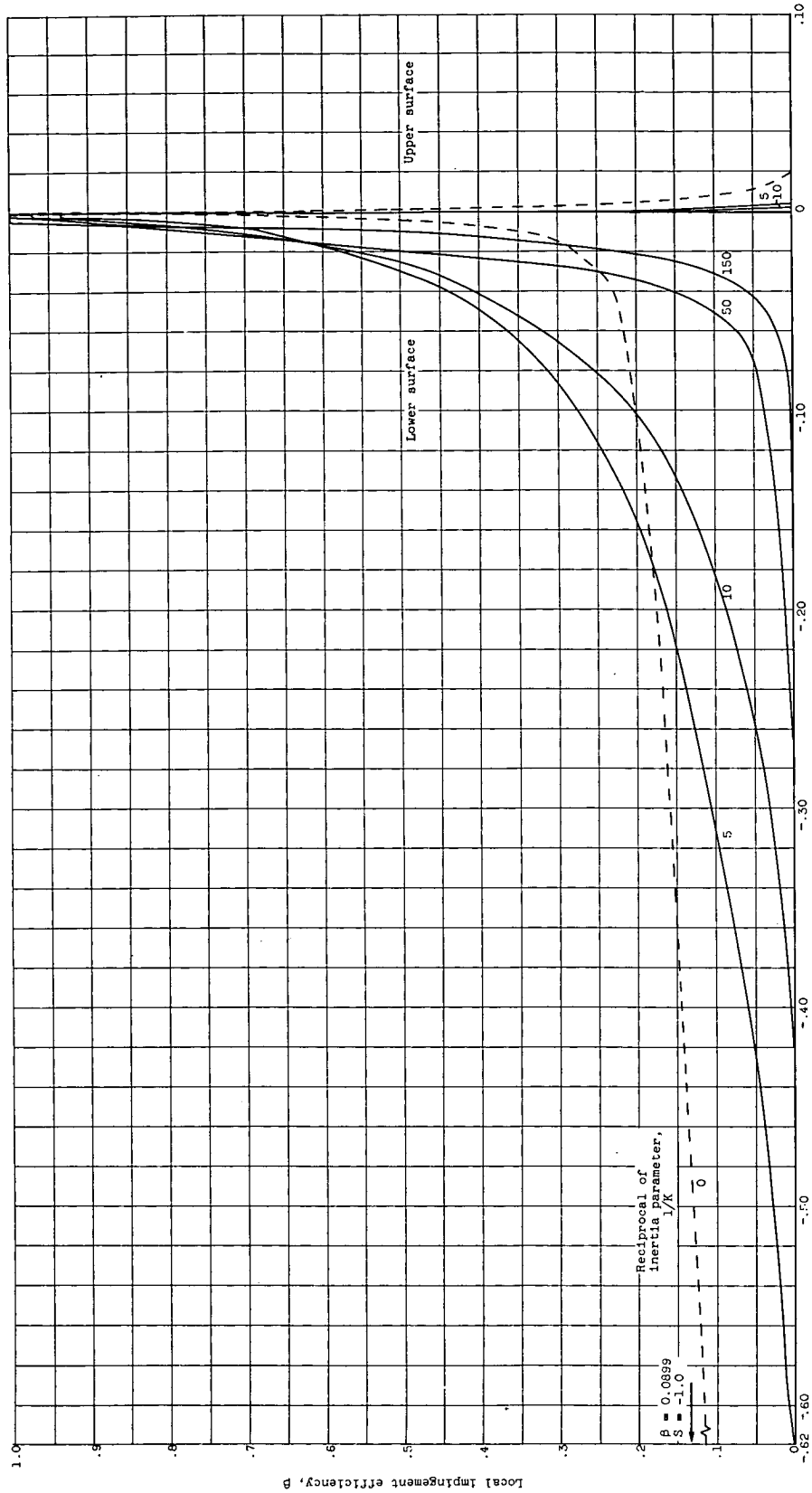
(c) Free-stream Reynolds number, 256.

Figure 7. - Continued. Trajectory starting ordinates as function of point of impingement on surface of 65A004 airfoil. Angle of attack, 8°.



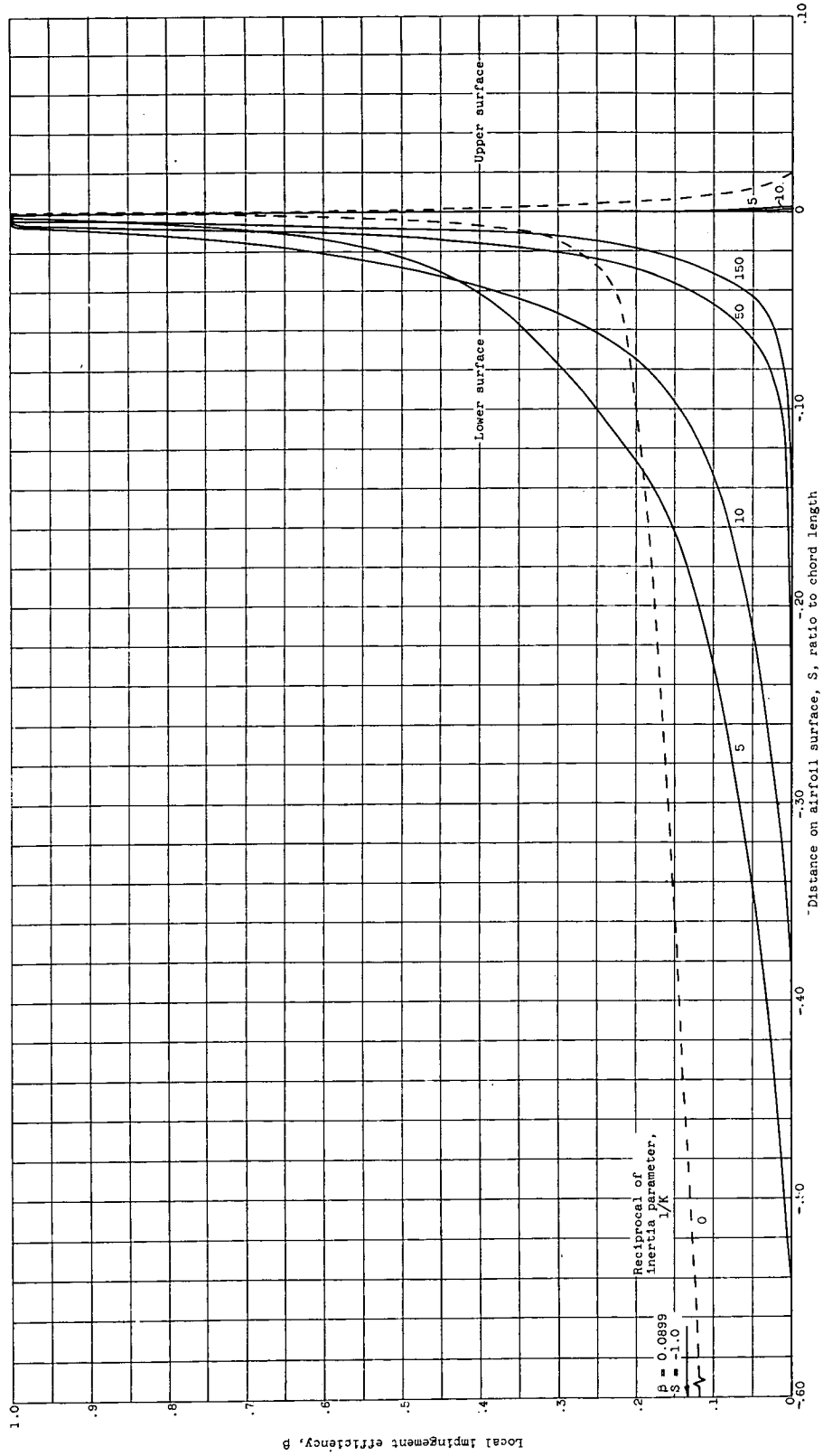
(d) Free-stream Reynolds number, 1024.

Figure 7. - Concluded. Trajectory starting ordinates as function of point of impingement on surface of 65A004 airfoil. Angle of attack, 8°.



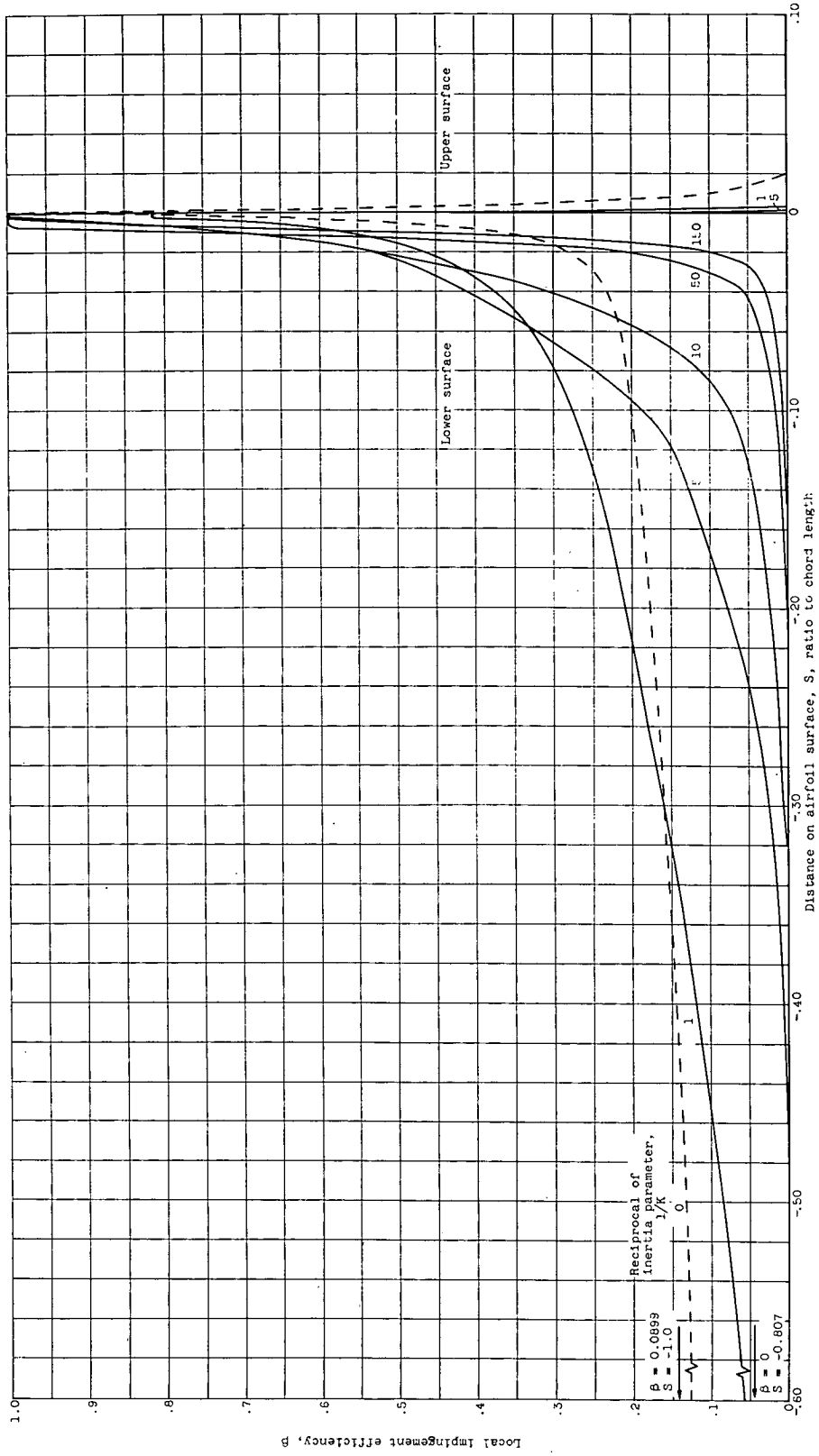
(a) Free-stream Reynolds number, 16.

Figure 8. - Local impingement efficiency of NACA 65A004 airfoil. Angle of attack, 8°.



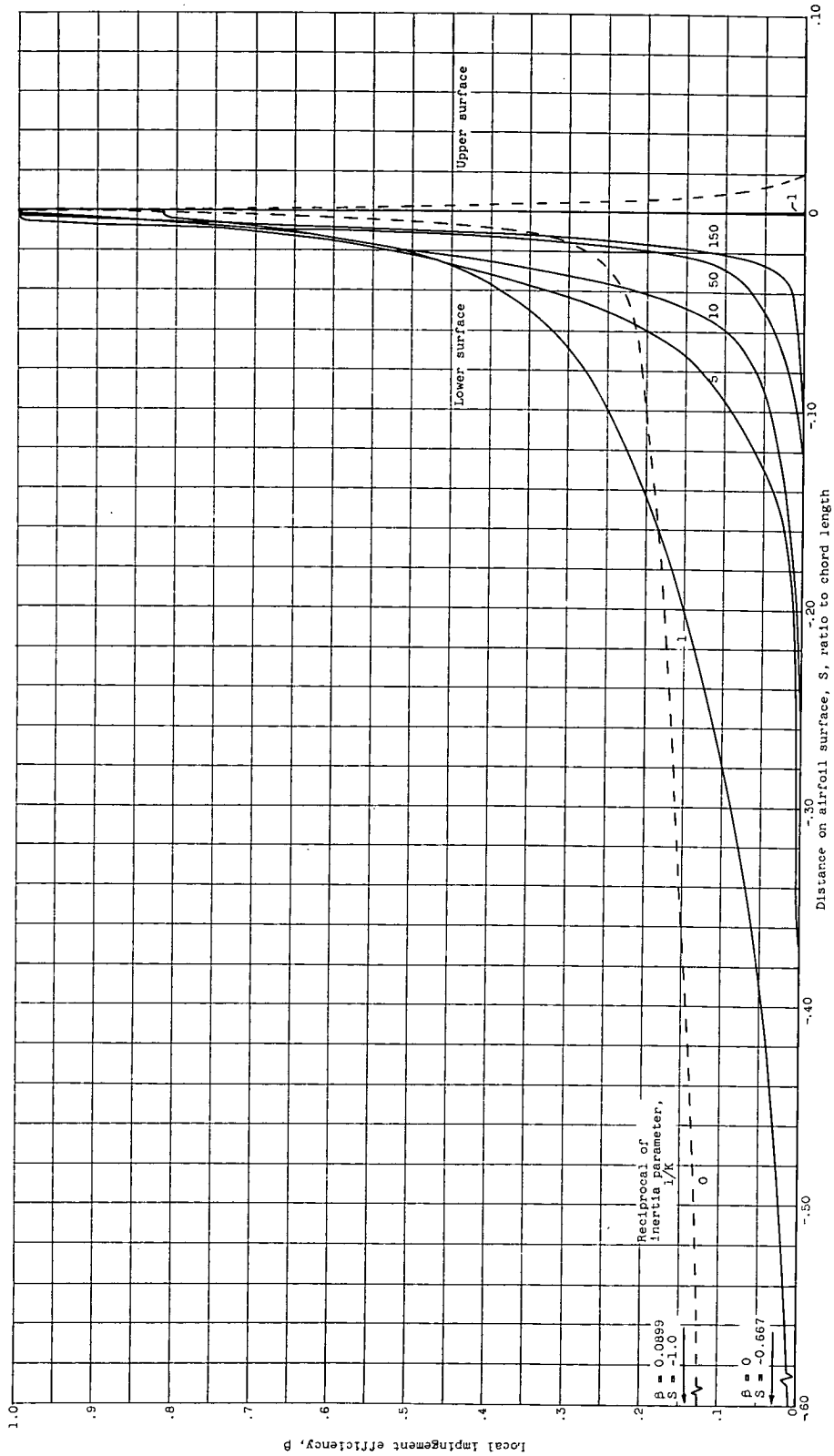
(b) Free-stream Reynolds number, 64.

Figure 8. - Continued. Local impingement efficiency of NACA 65A004 airfoil. Angle of attack, 8°.



(c) Free-stream Reynolds number, 256.

Figure 8. - Continued. Local impingement efficiency of NACA 65A004 airfoil. Angle of attack, 8°.



(d) Free-stream Reynolds number, 1024.

Figure 8. - Concluded. Local impingement efficiency of NACA 65A004 airfoil. Angle of attack, 8°.